A universal framework for nonlinear frequency combs under electro-optic modulation

Yanyun Xue[1,*], Xianpeng Lv[1,*], Guangxing Wu[2,*], Tianqi Lei[1,*], Chenyang Cao[1], Yiming Lei[1], Min Wang[1], Yan Li[1,3,4,5], Qihuang Gong[1,3,4,5], Di Zhu[2,†], Yaowen Hu[1,3,†]

[1]State Key Laboratory for Mesoscopic Physics and Frontiers Science Center for Nano-optoelectronics, School of Physics, Peking University, Beijing 100871, China
[2]Department of Materials Science and Engineering, National University of Singapore, Singapore 117575, Singapore
[3]Collaborative Innovation Center of Extreme Optics, Shanxi University, Taiyuan, China.
[4]Peking University Yangtze Delta Institute of Optoelectronics; Nantong 226010, China.
[5]Hefei National Laboratory; Hefei 230088, China.
[*]These authors contributed equally.
[†]Corresponding authors: dizhu@nus.edu.sg; yaowenhu@pku.edu.cn;

Nonlinear frequency combs, including electro-optic and Kerr combs, have become central platforms for chip-scale frequency synthesis. Recent breakthroughs in strong-coupling electro-optic modulation further expanded their accessible nonlinear dynamics, unlocking new phenomena and functionalities, but the underlying foundation remains largely unexplored. Here we establish a universal theoretical and experimental framework for nonlinear combs under arbitrary electro-optic modulation by introducing a general evolution equation (GEE) that transcends the mean-field Lugiato–Lefever equation. The GEE reduces to a discrete-time *Integration Hamiltonian* that provides a frequency-domain formalism unifying strong-coupling electro-optic modulation with photonic synthetic dimensions. Together with a band–wave correspondence linking modulation waveforms to synthetic band structures, the formalism enables programmable spectral control. We further show compatibility between Kerr nonlinearity and strong-coupling electro-optic modulation, highlighting their cooperative dynamics. Our work provides a foundational model for strong-coupling electro-optics in nonlinear combs, opening a route toward chip-integrated, microwave-programmable comb sources for metrology, spectroscopy, and emerging photonic technologies.

Introduction

Over the past two decades, nonlinear optical frequency combs in micro-resonators have reshaped modern photonics[1], enabling breakthroughs in optical communications[2,3], interconnects[4,5], computing[6–8], ranging[9–11] and precision metrology[12,13]. Among different implementations, Kerr combs have emerged as a leading platform, offering octave-spanning generation in compact, integrated devices[14,15]. Yet, they typically face a trade-off between repetition rate and spectral bandwidth[16], limiting scalability and flexibility. The advancement of the thin-film lithium niobate (TFLN)[17,18] has brought high-speed electro-optic (EO) modulation into this landscape, enabling comb generation with microwave-rate repetition and versatile spectral control. This progress has given rise to cavity EO[19–22] and hybrid EO–Kerr[23–26] combs. However, they are constrained by the relatively weak EO interaction and the stringent requirement of pump detuning control, with limited dynamical richness[16].

The recent emergence of strong-coupling EO modulation offers a promising pathway to overcome these challenges and to open new regimes for EO and hybrid EO–Kerr combs, where the EO-induced coupling strength exceeds the cavity's free spectral range. This regime unlocks a wealth of unexplored phenomena — from robust pump detuning with multi-pulse dynamics to fully programmable spectral shaping[27,28]. Beyond practical advantages, it also enriches the synthetic dimension and non-Hermitian physics[29–31], enabling phenomena such as multi-long-range interactions with a single-tone modulation and synthetic energy-band overlap, which are unattainable in weak-coupling regimes. Yet, despite this promise, previous models fail to explain these effects, nor the interplay between strong-coupling electro-optics and other optical nonlinearity including Kerr effect[30,31]. Developing a unified framework that captures nonlinear comb dynamics under arbitrary EO modulations is therefore crucial — not only to reveal the underlying new physics but also to guide the development of reconfigurable, high-bandwidth, and energy-efficient nonlinear comb sources for the next generation of optical and quantum technologies.

Here we address these challenges by establishing a universal theoretical and experimental framework for nonlinear frequency combs under EO modulation with arbitrary microwave waveforms and modulation strengths, which in particular extends to strong-coupling regimes. Central to this framework is a general evolution equation (GEE) that describes resonators in continuous time beyond the mean-field Lugiato–Lefever equation[32,33], enabling accurate modeling of EO modulation even in the presence of Kerr effects (Fig. 1a). Standing upon the recent development of discrete-time formalism attempted to describe this strong-coupling EO modulation[27] which lacks a well-defined Hamiltonian, we further show that for pure EO cavities the GEE reduces to a rigorous, discrete-time *Integration Hamiltonian* $\widehat{H}_{ig}$. It transcends

conventional tight-binding Hamiltonian and unifies frequency-domain mode coupling with the emerging synthetic dimension[29].

To demonstrate both generality and robustness, we experimentally validated the formalism on two complementary platforms: a fiber-cavity system and an integrated thin-film lithium niobate photonic circuit, bridging discrete-component and chip-integrated implementations. Within this framework, we uncover a fundamental band–wave correspondence (BWC), directly linking temporal modulation waveforms $V(t)$ to synthetic band structures $E(k)$, mediated by cavity dynamics in the detuning–angle (Δ, φ) parameter space (Fig. 1b). Leveraging these formalisms, we demonstrate tailored triangular-wave modulation to achieve independent EO comb sideband control, including single-sideband generation. Finally, by incorporating Kerr nonlinearity, we extend the framework and demonstrate soliton band-drifting that accommodates arbitrary waveform modulation and assists soliton addressing process. In particular, we report that strong-coupling enabled band overlap leads to EO pulse–Kerr soliton co-excitation, for the first time.

Introduction of general evolution equation

We first discuss the general evolution equation (GEE) that captures both the strong-coupling EO modulation and Kerr nonlinearity. When the pump power is sufficiently strong in a microwave-modulated resonator, the complete GEE yields:

$$\frac{da(\varphi,t)}{dt} = \left(-\frac{\kappa}{2} - i\Delta + i\Omega(\varphi,t)\right) a(\varphi,t) + \sqrt{\kappa_e}\, a_{in} t_R \delta\left(t - \frac{\varphi}{\omega_R}\right) + i\frac{D_2}{2}\frac{\partial^2}{\partial\varphi^2} a(\varphi,t) + ig|a(\varphi,t)|^2\, a(\varphi,t) \quad (1)$$

The coordinates (φ, t) represent the angle and time in the co-rotating frame, transformed from laboratory frame (φ', t') via: $\begin{cases} \varphi = \varphi' - \omega_R t' \\ t = t' \end{cases}$. The $a(\varphi,t)$ represents the annihilation operator of the azimuthal mode φ. The total loss rate is given by $\kappa = \kappa_i + \kappa_e$, where κ_i and κ_e are the internal and external loss rates, respectively. The angular frequencies of the center cavity mode and the pump are denoted by ω_0 and ω_p with $\Delta = \omega_0 - \omega_p$. Key cavity parameters include the repetition angular frequency ω_R, repetition rate f_R and round-trip period t_R. The modulation strength $\Omega(\varphi,t)$ is defined in terms of the local voltage as: $\Omega(\varphi,t) = \pi f_R \frac{V_{loc}(\varphi,t)}{\alpha V_\pi}$, here α is the modulation region ratio, V_π is the half-wave voltage, and $V_{loc}(\varphi,t) = V(t - \varphi/\omega_R)$, with $V(t)$ being the applied modulation wave. The dispersion coefficient is denoted by D_2 while the Kerr nonlinear coefficient is denoted by g.

The delta function $\delta\left(t-\frac{\varphi}{\omega_R}\right)=\delta\left((t-\frac{\varphi}{\omega_R})\ mod\ t_R\right)$ provides a periodic excitation. The periodic pump $\sqrt{\kappa_e}\,a_{in}t_R\delta\left(t-\frac{\varphi}{\omega_R}\right)$ introduced by GEE breaks the mean-field approximation and is the key advance for universal EO-modulated cavity modeling. It overcomes a fundamental flaw of the LLE: the mean-field approximation enforces an unphysical limit for repetition frequency $\omega_R{}'\to\infty$. This deficiency becomes critical under strong-coupling EO regime $\Omega_0=|\Omega(\varphi,t)|_{max}>\omega_R$ (Fig. 1a), leading to failure in both EO-dominated and EO–Kerr coexistent cavities. In particular, mean-field LLE simulation artificially reinjects pump energy at every step, imposing an artificial repetition frequency $\omega_R{}'\neq\omega_R$ and misrepresenting dynamics in the cavities. In contrast, GEE-based time evolution restores the natural t_R-periodic pump, potentially resolving the long-standing discrepancy between Kerr theory, simulations, and experiments (see details of GEE-based simulation methods in SI).

Formalism of *Integration Hamiltonian*

The periodic pump of GEE precludes stationary solutions in a continuous time scale. To connect the strong-coupling dynamics with synthetic dimension and non-Hermitian physics, we develop a simplified frequency-domain coupling-based Hamiltonian formalism for nonlinear systems with pure EO modulation, yielding discrete timescale stationary solutions. When Kerr nonlinearity is absent and dispersion is negligible[34], the simplified GEE in (1) yields: $\frac{da(\varphi,t)}{dt}=\left(-\frac{\kappa}{2}-i\Delta+i\Omega(\varphi,t)\right)a(\varphi,t)+\sqrt{\kappa_e}\,a_{in}t_R\delta\left(t-\frac{\varphi}{\omega_R}\right)$.

Experimental monitoring at the through port samples the field in the (φ,t) space along a specific trajectory: $\varphi(t)=-\omega_R t$ (equivalent to the fixed monitoring port in lab frame: $\varphi'=0$) (Fig. 1c). To predict field intensity of φ observed discrete times $t=-\varphi/\omega_R+nt_R(n\in\mathbb{Z})$, we derive a discrete-time Heisenberg equation (see SI for details):

$$\frac{\Delta a(\varphi,t)}{t_R}=i\left[\widehat{H}_{ig}(\varphi,t)/\hbar,a(\varphi,t)\right]-\frac{\kappa}{2}a(\varphi,t)+\sqrt{\kappa_e}a_{in} \tag{2}$$

Here $\Delta a(\varphi,t)=a(\varphi,t+t_R)-a(\varphi,t)$ defines field change between neighboring intersection points on this sampling trajectory. The *Integration Hamiltonian* $\widehat{H}_{ig}(\varphi,t)$ is derived from the integration of the GEE:

$$\widehat{H}_{ig}(\varphi,t)=i\hbar f_R\left(e^{\int_t^{t+t_R}(-i\Delta+i\Omega(\varphi,t))dt}-1\right)a^{\dagger}(\varphi,t)a(\varphi,t) \tag{3}$$

To model the dynamics directly in the spectral domain, we transform the *Integrated Hamiltonian* into the basis of longitudinal modes $\{a_\mu(t)\}$, where μ denotes the mode number (see SI for details):

$$\widehat{H}_{ig} = \sum_{\mu}\sum_{m} \hbar\left(W_m - if_R\delta_{0,m}\right) a_{\mu+m}(t)^\dagger a_\mu(t) \tag{4}$$

Where $\delta_{0,m}$ is the Kronecker delta. The coupling coefficients W_m are obtained from the Fourier series expansion of the transmission function: $T(\varphi) = if_R e^{\int_t^{t+t_R}(-i\Delta+i\Omega(\varphi,t))dt} = \sum_m W_m\, e^{im\varphi}$.

This spectral-domain formalism enables the direct calculation of EO comb spectra by solving the corresponding Heisenberg equations without invoking any rotating-wave approximation (RWA).

$$\frac{\Delta a_\mu(t)}{t_R} = i\left[\widehat{H}_{ig}/\hbar, a_\mu(t)\right] - \frac{\kappa}{2}a_\mu(t) + \sqrt{\kappa_e}a_{in}\,\delta_{0,\mu} \tag{5}$$

In contrast, applying the RWA in the continuous-time spectral-domain equations is mathematically equivalent to the mean-field approximation underlying the LLE—both approximations break down in the strong-coupling regime (see SI for details). For conventional single-sinusoidal modulation without detuning, we have

$$\begin{aligned}\widehat{H}_{ig} &= \frac{1}{2\pi}\int_0^{2\pi} i\hbar f_R\left(e^{i\Omega_0 cos(\varphi)/f_R} - 1\right)a^\dagger(\varphi,t)a(\varphi,t)d\varphi \\ &= \sum_{\mu}\sum_{m} i\hbar f_R\left(i^m J_m(\frac{\Omega_0}{f_R}) - \delta_{0,m}\right)a_{\mu+m}(t)^\dagger a_\mu(t)\end{aligned} \tag{6}$$

where J_m gives the m^{th} order Bessel function.

To verify such *Integration Hamiltonian* formalism, we perform experiments in two distinct platforms (fiber cavity and TFLN platform, Fig. 2a). We first show that the measured strong-coupling EO comb spectra agree well with the stationary state spectra directly solved by the Heisenberg equation from the $\widehat{H}_{ig}$ (Fig. 2b). Moreover, we perform a quantitative measure of the inter-mode coupling strength $|W_m|$ for m^{th} order governing energy transfer on the timescale of a cavity round-trip, consistent with $\widehat{H}_{ig}$ theoretical results (Fig. 2c).

Band-wave correspondence and direction-control of EO coupling

The discrete timescale *Integration Hamiltonian* requires a well-defined energy band. The excitation condition of mode φ is $\widehat{H}_{ig}(\varphi, t) = 0$, which defines a shifted eigenenergy $\omega_0 \rightarrow \omega_0(\varphi)$ for each mode yielding the energy band: $E(\varphi)/\hbar = \omega_0(\varphi) = \omega_0 - \pi f_R \frac{V(t=-\varphi/\omega_R)}{V_\pi} - n\omega_R$ (see SI for details). This expression establishes a direct band-wave correspondence (BWC): multiple ω_R-separated bands precisely replicate the shape of the modulation wave $V(t)$. We experimentally confirm this and observe that overlaps between these bands induce more than two pulses per round-trip (Fig. 3).

Leveraging the $\widehat{H}_{ig}$ and BWC, we engineer EO combs via synthetic band tailoring. We employ triangular waves as a basis. The modulation strength $\Omega_0 = \pi f_R \frac{|V_{max}|}{V_\pi}$ and asymmetry ratio $\gamma = \frac{t_{up}-t_{down}}{t_{up}+t_{down}}$ govern the comb properties (Fig. 4a). For symmetric triangular waves $(\gamma = 0)$, measured coupling spectra $|W_m| - m$ are symmetric and concentrated at a single dominant order $m_0 = 4\frac{\Omega_0}{\omega_R}$. This sharply contrasts with the diffuse, multi-order spectrum generated by sinusoidal driving, thereby highlighting the triangular wave's role as a fundamental modulation basis. Stronger modulation increases m_0, producing a clear spectral periodicity, as confirmed experimentally (Fig. 4b). For coupling spectra with $\gamma \in [-1,1]$, at extreme γ, one side exhibits strong low-order coupling, while the other shows only weak high-order coupling. Such directional coupling enhances energy flux in the preferred-coupling direction and produces a more prominent sideband, validated experimentally (Fig. 4c). This sideband asymmetry can also be explained by a band picture combining group velocity and density of states (see SI for details).

We achieve single-sideband control of the EO comb using triangular waves with tailored strength and asymmetry. This control arises because EO-comb dynamics are governed by the band slope near the excitation energy $\omega_0(\varphi) \sim \omega_p$, rather than the global wave. The nearly identical combs generated by a complete triangular wave and its peak-truncated variant (Fig. 4d) confirm the slope-dominant nature. Accordingly, single-sideband control is realized by tuning Ω_0 and asymmetry γ of triangular wave such that one slope near the excitation is preserved while the other is deliberately varied. Measured modulation waves and their spectra (Fig. 4e) verify the effectiveness of this approach.

Soliton band-drifting theory and deterministic Kerr solitons addressing

When an optical cavity is pumped with high power, Kerr nonlinearity should be considered adjointly with the EO effect. Based on the GEE, we introduce soliton band-drifting to describe dynamics involving multiple nonlinearities (Fig. 5a). The BWC principle remains valid here:

EO modulation distorts synthetic energy band $\omega_0(\varphi)$, deforms the modulation instability (MI) regime and confines all Kerr solitons to the red-detuning region $\omega_0(\varphi) > \omega_p$. A soliton at φ_0 drifts with velocity determined by the band slope $k = \partial\omega_0(\varphi_0)/\partial\varphi$. With a perturbative Lagrangian approach, we derive the soliton drifting velocity as (see Supplement)

$$v_d = \frac{d\varphi_0}{dt} = -\frac{d_2 k}{3},\ d_2 = 2D_2/\kappa. \tag{7}$$

Numerically simulated v_d results agree excellently with the theory (Fig. 5b).

To realize soliton addressing, a single soliton is stabilized at the band minimum ω_{0min}, while others emerging on band slope should be eliminated. The extra solitons drift toward band minimum ω_{0min} at velocity $v_d \propto -k$ while, during the detuning sweep, the MI boundary contracts in the same direction at $v_{MI} \propto -1/k$. Elimination occurs when solitons collide with MI boundaries, which requires a large slope k to satisfy $v_d > v_{MI}$.

Since the drifting velocity $|v_d| \propto (d_2 k)$, the addressing condition follows a complementary scaling law between d_2 and k. Increasing pump power P_{in} further reduces number of solitons, enhancing the addressing process. We quantify the probability of successful soliton addressing under sinusoidal modulation by sweeping (Ω_0, P_{in}) and (Ω_0, d_2) (Fig. 5c). Stronger EO modulation greatly alleviates the stringent requirements on dispersion and pump power, thereby enabling the realization of broad-span, low-repetition-rate combs.

By extending the two-dimensional space of (Ω_0, P_{in}), we identify distinct dynamical phases for sinusoidal modulation (Fig. 5d). To characterize each phase, we present detuning-angle Δ-φ diagrams that delineate the dynamical regimes, along with representative monitored pulse train power profiles (Fig. 5e). In particular, we show that strong-coupling enabled band overlap leads to EO pulse–Kerr soliton co-excitation, for the first time.

Conclusion and Outlook

In summary, we have established a universal framework for nonlinear frequency combs under strong-coupling EO modulation. The general evolution equation (GEE) provides a continuous-time description compatible with Kerr nonlinearities, while the reduced *Integration Hamiltonian* offers a frequency-domain formalism consistent with synthetic dimension approaches for EO-dominated cavities. Together, these models furnish a rigorous foundation for exploring topological and non-Hermitian dynamics[30,35–37] in strong-coupling EO combs. Experimental validation across both fiber-cavity and thin-film lithium niobate platforms confirms the universality of the framework from bulk to chip scale. Another central outcome of this work is

the band–wave correspondence (BWC), which directly links modulation waveforms to synthetic band structures. This principle opens an entirely new degree of freedom for synthetic band tailoring. Leveraging *Integration Hamiltonian* and BWC in combination, we demonstrate directional control of EO comb mode coupling with asymmetric triangular-wave modulation, enabling programmable spectrum shaping and single-sideband comb generation. Such asymmetric optical signal processing holds immediate promise for applications in sensing[38], FMCW LiDAR[39–41], optical communications[42–45], and dual-comb spectroscopy[46–49].

Beyond EO systems alone, the compatibility of the GEE with Kerr nonlinearity unlocks the possibility of strong-coupling EO–Kerr combs, which could combine the complementary advantages of EO precision and Kerr broadband solitons. Thin-film lithium niobate platforms[17,18]—already capable of realizing both EO[20,21] and Kerr combs[50–52]—provide a viable path toward achieving such hybrid systems experimentally. Future studies are expected to extend this approach to encompass more complex $\chi^{(2)}$ nonlinear effects—such as second-harmonic generation, optical parametric oscillation, and spontaneous parametric down-conversion—along with cascaded difference- and sum-frequency generation.

Our results therefore establish the first versatile and unified framework for strong-coupling EO combs, capturing universal dynamics in the presence of multiple nonlinearities. This framework may serve as a cornerstone for next-generation comb science and technology, enabling chip-integrated, microwave-programmable frequency comb sources with transformative opportunities for precision metrology[12,13], adaptive spectroscopy[46,53], optical communications[2,3,54], and emerging photonic computing[6–8,55].

References

1. Diddams, S. A., Vahala, K. & Udem, T. Optical frequency combs: Coherently uniting the electromagnetic spectrum. *Science* **369**, eaay3676 (2020).

2. Pfeifle, J. *et al.* Coherent terabit communications with microresonator Kerr frequency combs. *Nat. Photonics* **8**, 375–380 (2014).

3. Marin-Palomo, P. *et al.* Microresonator-based solitons for massively parallel coherent optical communications. *Nature* **546**, 274–279 (2017).

4. Rizzo, A. *et al.* Massively scalable Kerr comb-driven silicon photonic link. *Nat. Photonics* **17**, 781–790 (2023).

5. Rizzo, A. *et al.* Petabit-Scale Silicon Photonic Interconnects With Integrated Kerr Frequency Combs. *IEEE J. Sel. Top. Quantum Electron.* **29**, 1–20 (2023).

6. He, J. *et al.* Programmable electro-optic frequency comb empowers integrated parallel convolution processing. Preprint at https://doi.org/10.48550/arXiv.2506.18310 (2025).

7. Feldmann, J. *et al.* Parallel convolutional processing using an integrated photonic tensor core. *Nature* **589**, 52–58 (2021).

8. Xu, X. *et al.* 11 TOPS photonic convolutional accelerator for optical neural networks. *Nature* **589**, 44–51 (2021).

9. Trocha, P. *et al.* Ultrafast optical ranging using microresonator soliton frequency combs. *Science* **359**, 887–891 (2018).

10. Qi, Y. *et al.* 1.79-GHz acquisition rate absolute distance measurement with lithium niobate electro-optic comb. *Nat. Commun.* **16**, 2889 (2025).

11. Suh, M.-G. & Vahala, K. J. Soliton microcomb range measurement. *Science* **359**, 884–887 (2018).

12. Papp, S. B. *et al.* Microresonator frequency comb optical clock. *Optica* **1**, 10 (2014).

13. Niu, R. *et al.* An integrated wavemeter based on fully-stabilized resonant electro-optic frequency comb. *Commun. Phys.* **6**, 329 (2023).

14. Kippenberg, T. J., Gaeta, A. L., Lipson, M. & Gorodetsky, M. L. Dissipative Kerr solitons in optical microresonators. *Science* **361**, eaan8083 (2018).

15. Shen, B. *et al.* Integrated turnkey soliton microcombs. *Nature* **582**, 365–369 (2020).

16. Chang, L., Liu, S. & Bowers, J. E. Integrated optical frequency comb technologies. *Nat. Photonics* **16**, 95–108 (2022).

17. Zhu, D. *et al.* Integrated photonics on thin-film lithium niobate. *Adv. Opt. Photonics Vol 13 Issue 2 Pp 242-352* https://doi.org/10.1364/AOP.411024 (2021) doi:10.1364/AOP.411024.

18. Hu, Y. *et al.* Integrated electro-optics on thin-film lithium niobate. *Nat. Rev. Phys.* **7**, 237–254 (2025).

19. Rueda, A., Sedlmeir, F., Kumari, M., Leuchs, G. & Schwefel, H. G. L. Resonant electro-optic frequency comb. *Nature* **568**, 378–381 (2019).

20. Zhang, M. *et al.* Broadband electro-optic frequency comb generation in a lithium niobate microring resonator. *Nature* **568**, 373–377 (2019).

21. Hu, Y. *et al.* High-efficiency and broadband on-chip electro-optic frequency comb generators. *Nat. Photonics* **16**, 679–685 (2022).

22. Zhang, J. *et al.* Ultrabroadband integrated electro-optic frequency comb in lithium tantalate. *Nature* **637**, 1096–1103 (2025).

23. Song, Y., Hu, Y., Lončar, M. & Yang, K. Hybrid Kerr-electro-optic frequency combs on thin-film lithium niobate. *Light Sci. Appl.* **14**, 270 (2025).

24. Englebert, N. *et al.* Bloch oscillations of coherently driven dissipative solitons in a synthetic dimension. *Nat. Phys.* **19**, 1014–1021 (2023).

25. Tusnin, A. K., Tikan, A. M. & Kippenberg, T. J. Nonlinear states and dynamics in a synthetic frequency dimension. *Phys. Rev. A* **102**, 023518 (2020).

26. Wan, S. *et al.* Self-locked broadband Raman-electro-optic microcomb. *Nat. Commun.* **16**, 4829 (2025).

27. Lei, T. *et al.* Strong-coupling and high-bandwidth cavity electro-optic modulation for advanced pulse-comb synthesis. *Light Sci. Appl.* **14**, 373 (2025).

28. Song, Y. *et al.* Universal dynamics and microwave control of programmable cavity electro-optic frequency combs. Preprint at https://doi.org/10.48550/arXiv.2507.21835 (2025).

29. Dutt, A. *et al.* Experimental band structure spectroscopy along a synthetic dimension. *Nat. Commun.* **10**, 3122 (2019).

30. Wang, K. *et al.* Generating arbitrary topological windings of a non-Hermitian band. *Science* **371**, 1240–1245 (2021).

31. Wang, K., Dutt, A., Wojcik, C. C. & Fan, S. Topological complex-energy braiding of non-Hermitian bands. *Nature* **598**, 59–64 (2021).

32. Lugiato, L. A., Prati, F., Gorodetsky, M. L. & Kippenberg, T. J. From the Lugiato–Lefever equation to microresonator-based soliton Kerr frequency combs. *Philos. Trans. R. Soc. Math. Phys. Eng. Sci.* **376**, 20180113 (2018).

33. Lugiato, L. A. & Lefever, R. Spatial Dissipative Structures in Passive Optical Systems. *Phys. Rev. Lett.* **58**, 2209–2211 (1987).

34. Tidy3D simulation project. https://www.flexcompute.com/tidy3d/community/notebooks/DispersionAnalysisEOComb/. (2025).

35. Li, G. *et al.* Direct extraction of topological Zak phase with the synthetic dimension. *Light Sci. Appl.* **12**, 81 (2023).

36. Yu, D., Peng, B., Chen, X., Liu, X.-J. & Yuan, L. Topological holographic quench dynamics in a synthetic frequency dimension. *Light Sci. Appl.* **10**, 209 (2021).

37. Song, W. *et al.* Breakup and Recovery of Topological Zero Modes in Finite Non-Hermitian Optical Lattices. *Phys Rev Lett* **123**, 165701 (2019).

38. Feng, H. *et al.* On-chip optical vector analysis based on thin-film lithium niobate single-sideband modulators. *Adv. Photonics* **6**, (2024).

39. Kamata, M., Hinakura, Y. & Baba, T. Carrier-Suppressed Single Sideband Signal for FMCW LiDAR Using a Si Photonic-Crystal Optical Modulators. *J. Light. Technol. Vol 38 Issue 8 Pp 2315-2321* https://opg.optica.org/jlt/abstract.cfm?uri=jlt-38-8-2315 (2020).

40. Shi, P. *et al.* Optical FMCW Signal Generation Using a Silicon Dual-Parallel Mach-Zehnder Modulator. *IEEE Photonics Technol. Lett.* **33**, 301–304 (2021).

41. Dong, Y., Zhu, Z., Tian, X., Qiu, L. & Ba, D. Frequency-Modulated Continuous-Wave LIDAR and 3D Imaging by Using Linear Frequency Modulation Based on Injection Locking. *J. Light. Technol.* **39**, 2275–2280 (2021).

42. Bo, T., Kim, H., Tan, Z. & Dong, Y. Optical Single-Sideband Transmitters. *J. Light. Technol.* **41**, 1163–1174 (2023).

43. Wang, Y. *et al.* Ultra-wideband microwave photonic frequency downconverter based on carrier-suppressed single-sideband modulation. *Opt. Commun.* **410**, 799–804 (2018).

44. Xie, X. *et al.* Broadband Millimeter-Wave Frequency Mixer Based on Thin-Film Lithium Niobate Photonics. *Electromagn. Sci.* **3**, 0090462-1-0090462–10 (2025).

45. Paloi, F. & Haxha, S. Analysis of the carrier suppressed single sideband modulation for long distance optical communication systems. *Optik* **161**, 230–243 (2018).

46. Ideguchi, T., Poisson, A., Guelachvili, G., Picqué, N. & Hänsch, T. W. Adaptive real-time dual-comb spectroscopy. *Nat. Commun.* **5**, 3375 (2014).

47. Coddington, I., Newbury, N. & Swann, W. Dual-comb spectroscopy. *Optica* **3**, 414 (2016).

48. Dutt, A. *et al.* On-chip dual-comb source for spectroscopy. *Sci. Adv.* **4**, e1701858 (2018).

49. Suh, M.-G., Yang, Q.-F., Yang, K. Y., Yi, X. & Vahala, K. J. Microresonator soliton dual-comb spectroscopy. *Science* **354**, 600–603 (2016).

50. Song, Y., Zhu, X., Zuo, X., Huang, G. & Lončar, M. Stable gigahertz- and mmWave-repetition-rate soliton microcombs on X-cut lithium niobate. *Optica* **12**, 693 (2025).

51. Song, Y., Hu, Y., Zhu, X., Yang, K. & Lončar, M. Octave-spanning Kerr soliton frequency combs in dispersion- and dissipation-engineered lithium niobate microresonators. *Light Sci. Appl.* **13**, 225 (2024).

52. Lv, X. *et al.* Broadband microwave-rate dark pulse microcombs in dissipation-engineered LiNbO3 microresonators. *Nat. Commun.* **16**, 2389 (2025).

53. Yasui, T. *et al.* Adaptive sampling dual terahertz comb spectroscopy using dual free-running femtosecond lasers. *Sci. Rep.* **5**, 10786 (2015).

54. Fortier, T. & Baumann, E. 20 years of developments in optical frequency comb technology and applications. *Commun. Phys.* **2**, 153 (2019).

55. Pfister, O. Continuous-variable quantum computing in the quantum optical frequency comb. *J. Phys. B At. Mol. Opt. Phys.* **53**, 012001 (2020).

Acknowledgements: Y.X. acknowledges Qixuan Zhou, Cheng Wang, Hanfei Hou, Tong Ge, Junting Bie for helpful discussion. Y.X. acknowledges Hang Yuan, Fan Yang for administrative support, as well as Tom Chen (Flexcompute).

Author contributions: Y.X., T.L., and Y.H. conceived the project and contributed to theoretical modeling. X.L. constructed the fiber cavity. G.W. fabricated the TFLN chip. Y.X. and T.L. performed the measurement. Y.X. performed the numerical simulations, and data processing. Y.X. and Y.H. wrote the manuscript with input from all authors. C.C., Y.L. and M.W. helped the project. Y.H., D.Z., Q.G. and Y.L. supervised the project.

Funding: This research is supported by the National Key Research and Development Program (2023YFB3211200), Quantum Science and Technology-National Science and Technology Major Project (2024ZD0302500, 2024ZD0302501, 2024ZD0301600), National Science Foundation of China (NSFC-12474321), National Research Foundation Singapore (NRF-NRFF15-2023-0005).

Competing interests: The authors declare no competing interests.

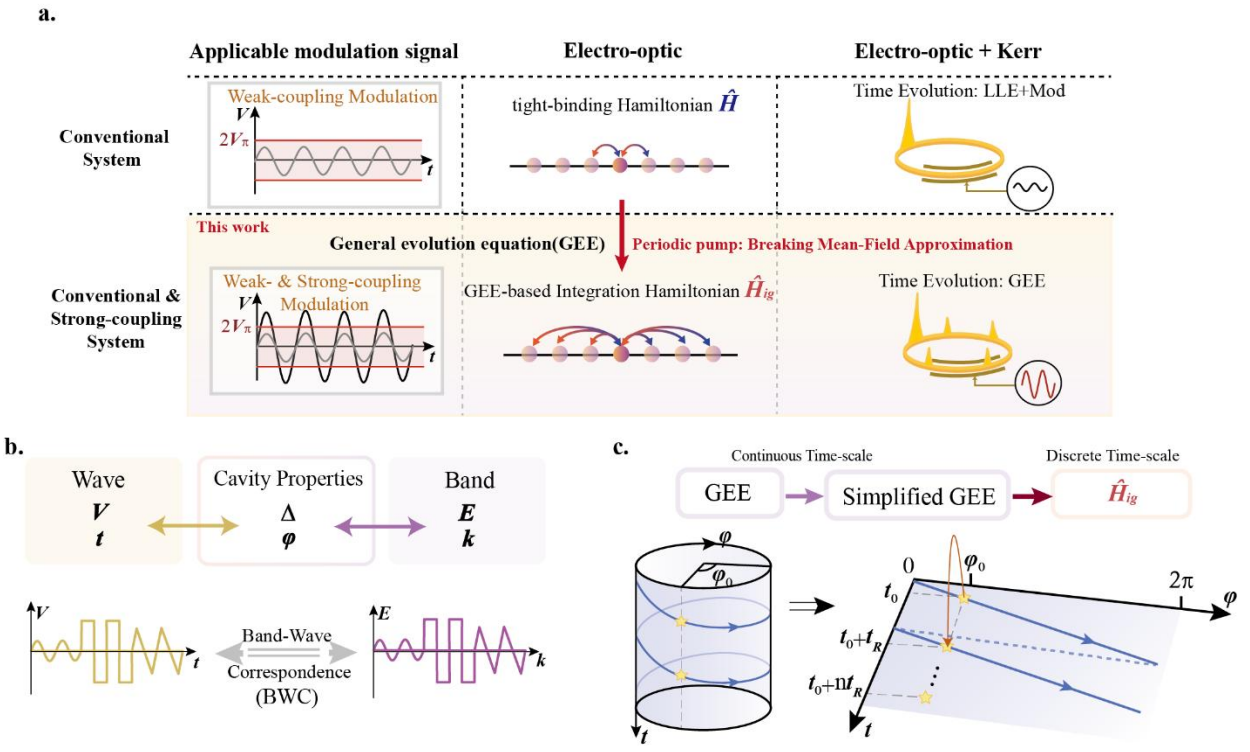

Figure 1 | Nonlinear system under strong-coupling electro-optic (EO) modulation with general evolution equation (GEE) and band-wave correspondence (BWC). a, GEE breaks the mean-field approximation by introducing the periodic pump, allowing unified framework for EO– and EO–Kerr system in both weak- and strong-coupling regime. **b,** The synthetic dimensional band structure ($E-k$) corresponds to the modulation wave ($V-t$), linked through resonator dynamics in the parameter space of detuning-angle ($\Delta-\varphi$). **c,** In EO-dominated, low power cavities, the GEE reduces to a simplified term, and further to the *Integration Hamiltonian* which captures stationary solutions on a discrete time-scale. In optical cavities, the angle φ and time t define a cylindrical parameter space. Experimental monitoring samples the space along the trajectory $\varphi(t) = -\omega_R t$ (blue line). For an azimuthal mode φ_0 observed at discrete times $t_0 + nt_R, n \in \mathbb{Z}$, the discrete-time Heisenberg equation of motion defines the *Integration Hamiltonian* $\widehat{H}_{ig}$, from which the corresponding energy band structure $E(k)$ with quasi-momentum $k = \varphi$ can be derived.

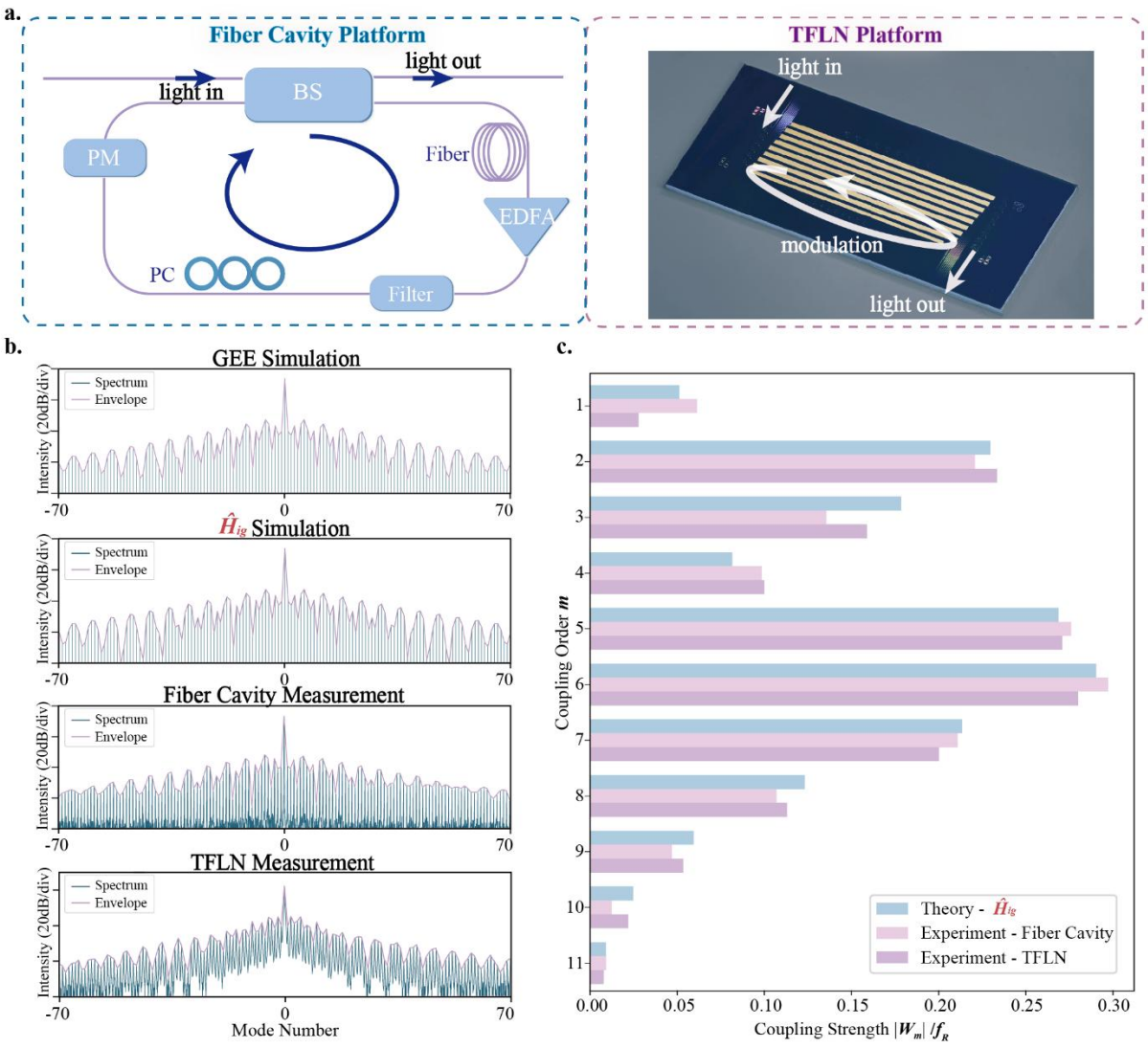

Figure 2 | Formalism of *Integration Hamiltonian*. a, Illustration of the experiment platforms. Left: fiber cavity platform; PC, polarization controller; PM, phase modulator; BS, beam splitter; EDFA, erbium doped fiber amplifier. Right: Thin-film lithium niobate (TFLN) photonics chip, with fiber-fiber coupling configuration. **b,** Simulated and measured spectra under microwave drive $|V_{max}| = 2.3V_\pi$ $(\Omega_0 = 1.15\omega_R)$. **c,** The measured and calculated coupling intensities $|W_m| - m$ for the *Integration Hamiltonian*.

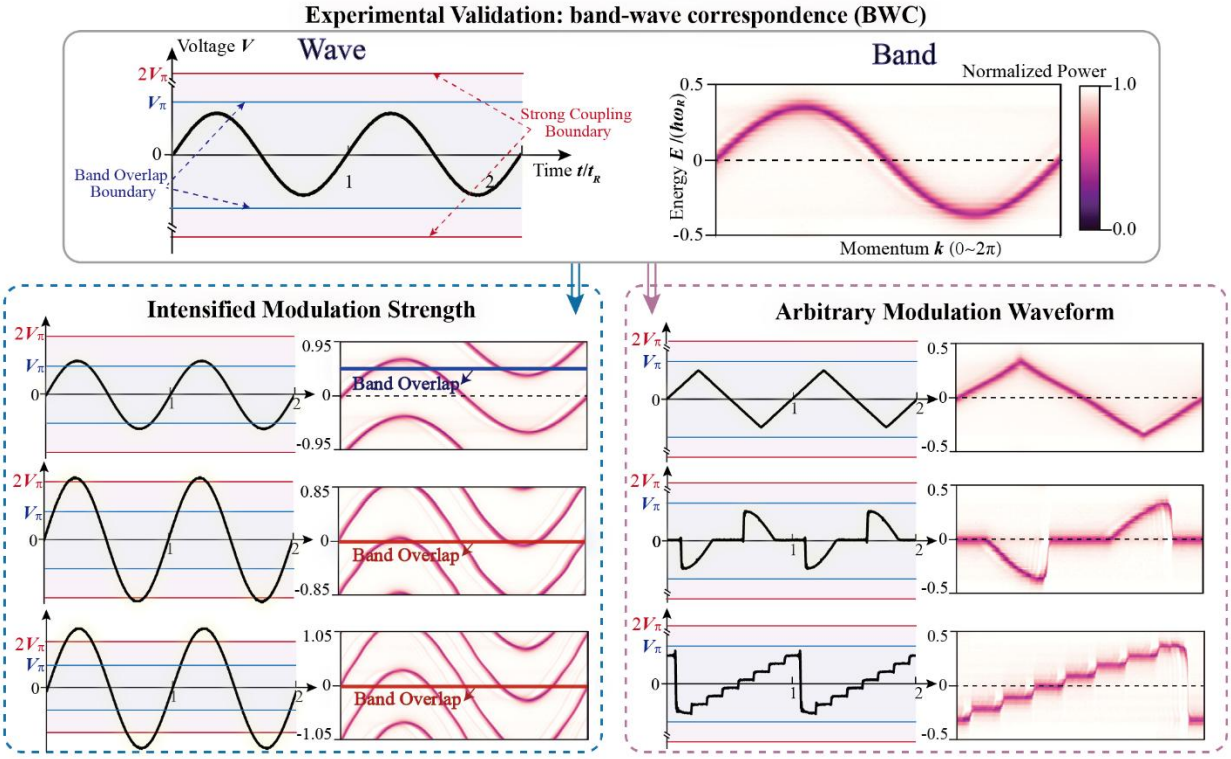

Figure 3 | Experimental demonstration of band-wave correspondence (BWC). Measured modulation waveform and corresponding band structure in a fiber cavity, validating the BWC principle at arbitrary modulation strength and waveform. With increasing modulation strength, beyond the band overlap boundary $|V_{max}| > V_\pi$ (blue boundary), band overlaps happen at $\Delta \neq 0$; beyond the strong-coupling boundary $|V_{max}| > 2V_\pi$ (red boundary), band overlaps happen at $\Delta = 0$.

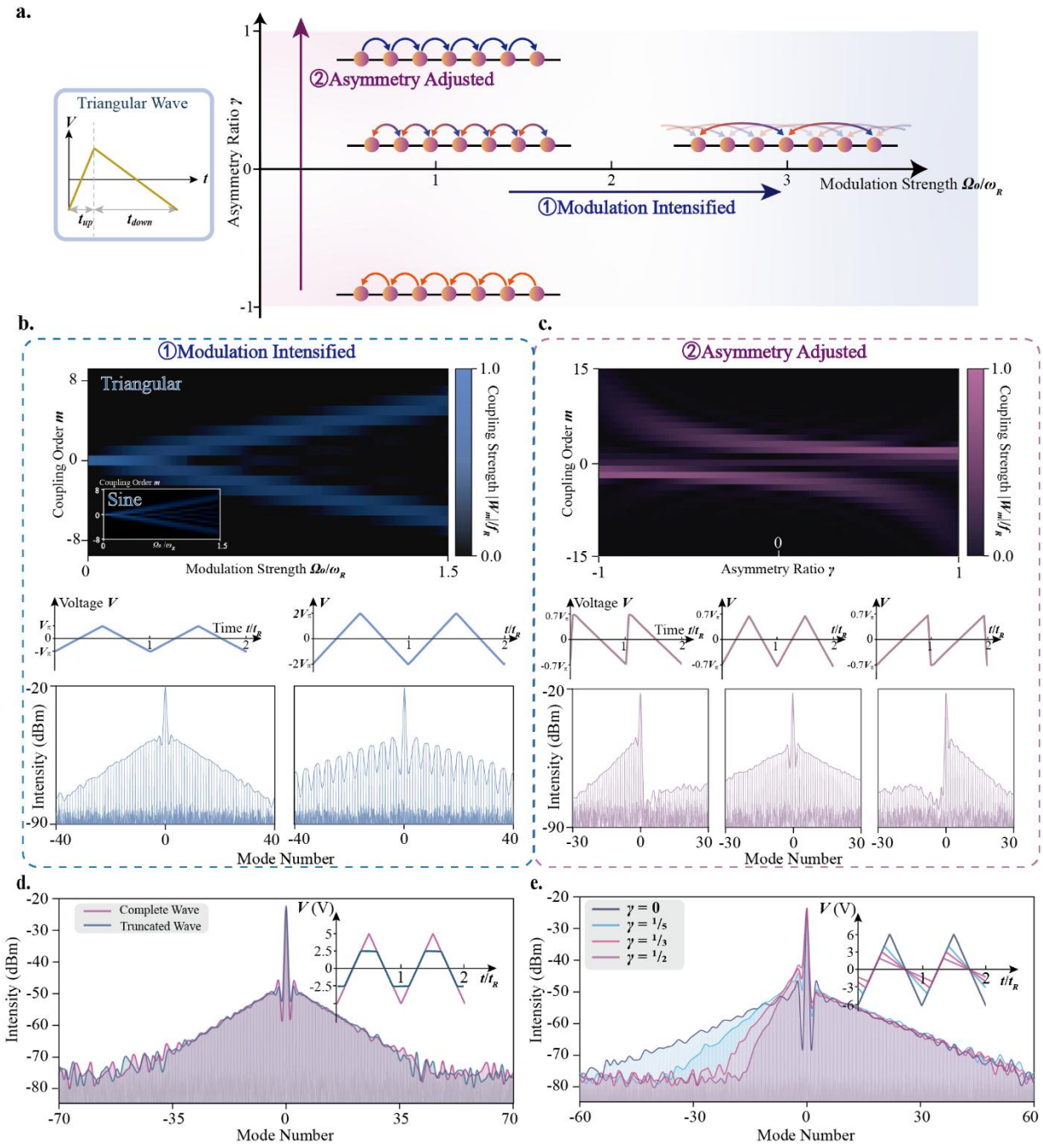

Figure 4 | EO combs: Triangular waveform as sideband engineering enabler. a, The triangular modulation, characterized by modulation strength Ω_0 and asymmetry γ enables engineering of EO comb frequency-domain mode coupling. **b,** Coupling strength spectrum $|W_m| - m$ as a function of Ω_0. Inset: corresponding spectrum under sinusoidal wave modulation. Experiments confirm that increasing Ω_0 elevates the coupling order in EO comb spectra. **c,** Coupling strength spectrum $|W_m| - m$ as a function of γ. Experiments confirm that this directional coupling enhances the sideband in the strongly coupled direction. **d,** Experiments confirm that EO comb dynamics are governed by band slope near the excitation energy ω_p. **e,** Experimental demonstration of unidirectional EO comb control with strength-asymmetry-tailored triangular wave.

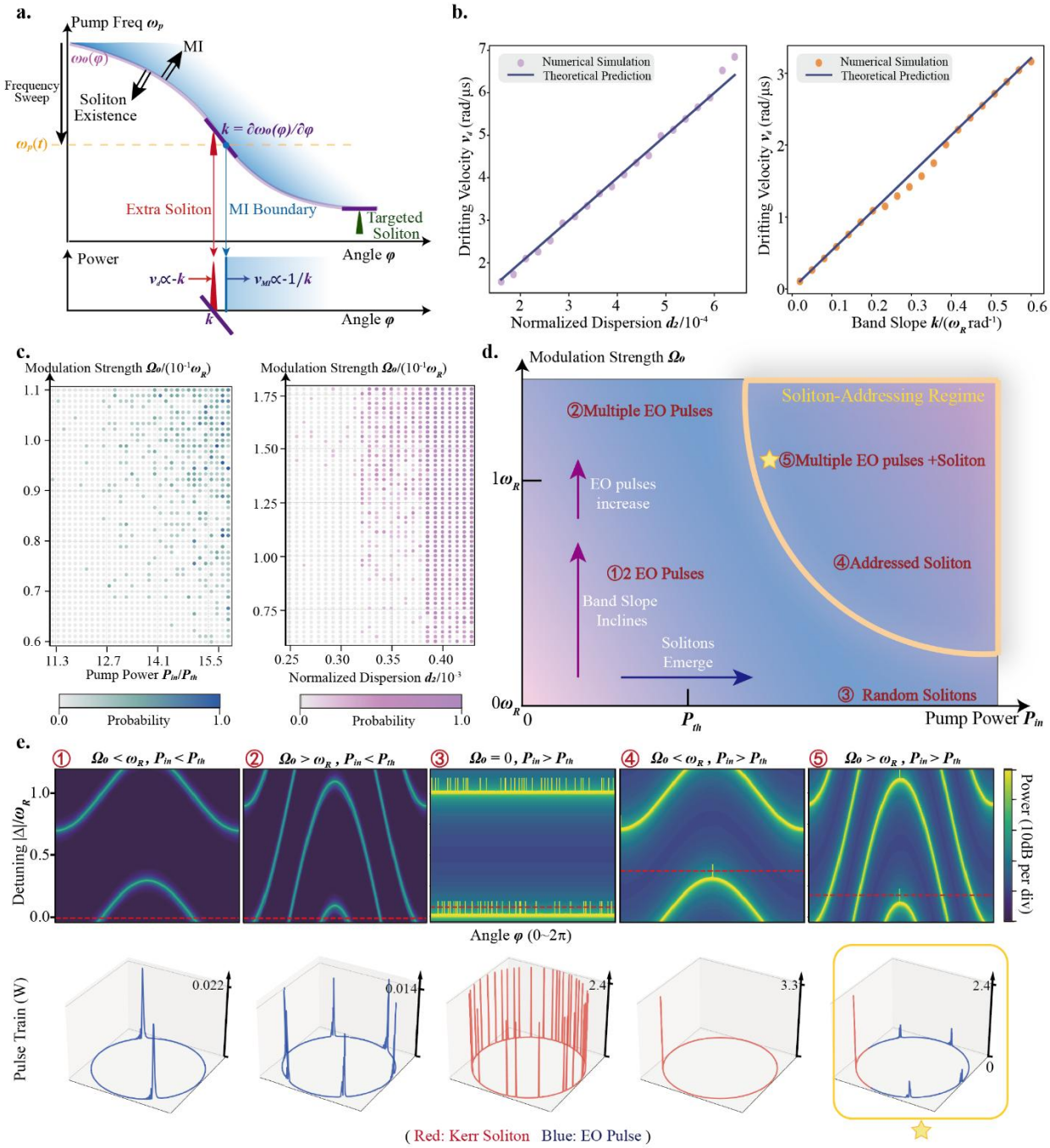

Figure 5 | Soliton band-drifting theory and strong-coupling EO–Kerr phenomena. a, Schematic of soliton band-drifting dynamics and soliton-addressing conditions. Under coexistence of Kerr nonlinearity and EO effect, in a blue-to-red frequency sweep, the parameter space of pump frequency ω_p and angle φ separates into soliton-existence and modulation-instability (MI) regimes, divided by a curve parallel to the energy band $\omega_0(\varphi)$. Soliton addressing is achieved when extra solitons emerging at non-zero band slope k drift and collide with MI boundary, requiring larger band slopes k and modulation strengths Ω_0. **b,** Numerical simulation results of drifting velocity v_d with band slope k and normalized dispersion $d_2 = \frac{2D_2}{\kappa}$. **c,** Probability of successful soliton addressing is quantified by sweeping Ω_0, d_2 and pump power P_{in} (P_{th} is the threshold power of parametric oscillation). **d,** Phase diagram of

cavity states under sinusoidal wave modulation in two-dimensional space of (Ω_0 , P_{in}). The soliton-addressing regime defines the conditions for soliton addressing. **e,** Detailed phase conditions and representative monitored pulse-train dynamics (at selected detunings denoted by red horizontal lines). We have used a moderate intrinsic quality factor $Q_i = 1 \times 10^6$ for TFLN to perform simulations.